Quantum Critical Transition Amplifies Magnetoelastic Coupling in $Mn[N(CN)_2]_2$

T. V. Brinzari,[1] P. Chen,[1] Q.-C. Sun,[1] J. Liu,[2] L.-C. Tung,[3,*] Y. Wang,[3] J. A. Schlueter,[4] J. Singleton,[5] J. L. Manson,[6] M.-H. Whangbo,[2] A. P. Litvinchuk,[7] and J. L. Musfeldt[1]

[1]*Department of Chemistry, University of Tennessee, Knoxville, Tennessee 37996, USA*
[2]*Department of Chemistry, North Carolina State University, Raleigh, North Carolina 27695-8204, USA*
[3]*National High Magnetic Field Laboratory, Tallahassee, Florida 32310, USA*
[4]*Materials Science Division, Argonne National Laboratory, Argonne, Illinois 60439, USA*
[5]*National High Magnetic Field Laboratory, Los Alamos National Laboratory, Los Alamos, New Mexico 87545, USA*
[6]*Department of Chemistry and Biochemistry, Eastern Washington University, Cheney, Washington 99004, USA*
[7]*Texas Center for Superconductivity and Department of Physics, University of Houston, Houston, Texas 77204, USA*

(Received 25 January 2013; published 5 June 2013)

We report the discovery of a magnetic quantum critical transition in $Mn[N(CN)_2]_2$ that drives the system from a canted antiferromagnetic state to the fully polarized state with amplified magnetoelastic coupling as an intrinsic part of the process. The local lattice distortions, revealed through systematic phonon frequency shifts, suggest a combined MnN_6 octahedra distortion + counterrotation mechanism that reduces antiferromagnetic interactions and acts to accommodate the field-induced state. These findings deepen our understanding of magnetoelastic coupling near a magnetic quantum critical point and away from the static limit.

DOI: 10.1103/PhysRevLett.110.237202 PACS numbers: 75.50.Xx, 63.70.+h, 75.30.Kz, 75.80.+q

Quantum phase transitions and associated quantum critical points present a rich and challenging research area that is of current fundamental interest [1]. In contrast to classical phase transitions governed by thermal fluctuations, quantum phase transitions are driven by an external parameter such as magnetic field, pressure, or composition [1]. One case where field works as a quantum tuning parameter is in the suppression of antiferromagnetic order by applied magnetic field where the resulting quantum critical point separates the antiferromagnetic state from the fully polarized paramagnetic state [2–4]. This and other more complicated magnetically driven transitions [5–7] are of foundational importance to the field of quantum magnetism, yet due to energy scale considerations, real physical systems can be challenging to identify. Molecule-based materials offer a way forward. Their low magnetic energy scales are well-suited for investigating magnetically driven transitions, and their chemical flexibility and softness offer opportunities to tune properties and couple functionality [3,4,8]. $Mn[N(CN)_2]_2$ attracted our attention in this regard [9,10]. What distinguishes this work from previous efforts to investigate magnetoelastic coupling [4] is the three dimensionality of this system, the lack of hydrogen bonding, and easy access to the long-range ordered state.

In this Letter, we report the discovery of a magnetic quantum critical transition in $Mn[N(CN)_2]_2$, the complete magnetic field-temperature phase diagram, and enhanced magnetoelastic coupling through the field-driven transition that we analyze in terms of local lattice distortions. The latter reveals a combined MnN_6 octahedra distortion + counterrotation mechanism that reduces antiferromagnetic interactions and stabilizes the fully polarized state. Similar local lattice distortions and exchange pathways underpin the remarkable properties of photomagnetic cyanides, ferroelectrics, and correlated oxides [11,12]. These findings advance the fundamental understanding of quantum phase transitions, provide insight into higher energy scale materials [13], and are relevant to more complicated processes in which magnetic field acts as a tuning parameter including multiferroicity [14], multiple magnetization plateaus [5,6], and skyrmion lattice development [7].

Powdered $Mn[N(CN)_2]_2$ was prepared as described in Ref. [9], and isothermal magnetization was measured using a 65 T short-pulse magnet located at the National High Magnetic Field Laboratory (NHMFL) [3]. Variable temperature and field spectroscopies were performed in our own lab and at the NHMFL (30–3500 cm^{-1}, 4.2–300 K, 0–35 T, 0.3–1 cm^{-1} resolution). Density functional calculations were used to expose various properties including lattice vibrations and spin densities [15].

Figure 1(a) displays the isothermal magnetization of $Mn[N(CN)_2]_2$ below the antiferromagnetic transition temperature $T_N = 15.85$ K as a function of magnetic field up to 51 T. The 0.5 K data show a linear increase with field above the 0.48 T spin flop transition [10] and a sharp, elbowlike transition to saturation at $B_c = 30.4 \pm 0.1$ T after which the fully polarized state is achieved. The 4 K data have a similar profile and a 29.8 ± 0.2 T critical field. This behavior is a signature of a magnetic quantum phase transition [2,3]; that it occurs at experimentally realizable fields makes it especially attractive. We use mean field theory to relate the critical field (B_c) to the exchange interaction as $g\mu_B B_c = |n(2JS)|$, where $S = 5/2$ for Mn^{2+}, $n = 8$ is the number of nearest neighbors, $g = 2.0$, and μ_B is the Bohr magneton. We find $J/k_B \leq -1.0$ K, which compares well with the estimate of $J/k_B = -0.78$ K from specific heat

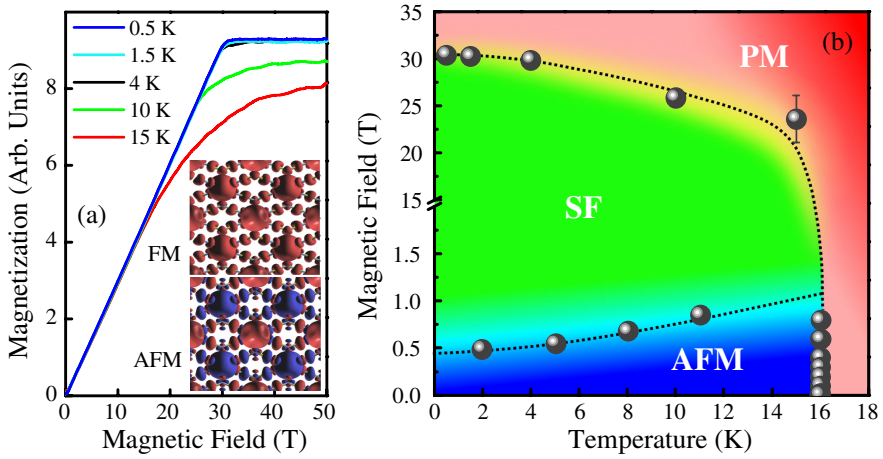

FIG. 1 (color online). (a) Isothermal magnetization of $Mn[N(CN)_2]_2$. Inset: calculated spin density distribution for antiferromagnetic and ferromagnetic states of $Mn[N(CN)_2]_2$. (b) Comprehensive B-T phase diagram displaying antiferromagnetic [AFM (canting angle is small [10])], spin-flop (SF), and paramagnetic (PM) phases. High-field data points are taken as the midpoints of the transition. Low-field data points are from Ref. [10]. The colors and dashed lines guide the eye.

measurements [10,16]. Bringing the extracted critical fields together with previously published work [10] allows us to construct the B-T phase diagram [Fig. 1(b)]. Interestingly, a single value of J cannot simultaneously account for both magnetic energy scales in this system ($T_N = 15.85$ K and $B_c = 30.4$ T). Possible origins of this discrepancy include beyond mean field corrections [17] or a field-dependent exchange interaction [5]. Spin density calculations reveal an out-of-phase pattern in the low-field antiferromagnetic state and a uniform density in the high-field state (Fig. 1), with the majority of spin density on the Mn sites in each case.

Figure 2(a) displays the far infrared absorption spectrum of $Mn[N(CN)_2]_2$ at 4.2 K. On the basis of our first-principles lattice dynamics calculations and a literature comparison [18], we assign the peaks at 79 and 108 cm^{-1} to lattice modes with dominant Mn displacement, phonons at 162/167 and 194 cm^{-1} to NMnN bending, features between 220 and 300 cm^{-1} to Mn-N stretching modes + ligand bands, and peaks at around 500 cm^{-1} to NCN in- and out-of plane bending. A complete spectrum and assignment are available in [15]. The magnetoinfrared response of $Mn[N(CN)_2]_2$ reveals remarkable sensitivity to the quantum critical transition. To emphasize spectral changes through B_c, we calculate the full field absorption difference spectrum $\Delta\alpha = \alpha(B = 35\ \text{T}) - \alpha(0\ \text{T})$ [Fig. 2(b)]. This difference simultaneously highlights striking change and rigid behavior. The exact course of each mode depends on the precise nature of its displacement pattern. Moreover, the field-dependent features either soften or harden systematically with field, a trend that again correlates with the detailed mode motion. In fact, at heart, $\Delta\alpha$ changes reflect frequency shifts as evidenced by the symmetric derivative-like structures in the absorption difference spectrum. As an example, Fig. 2(c) displays a close-up view of the absorption difference spectrum for the two low-frequency Mn displacement modes. The magnitude of $\Delta\alpha$ increases continuously due to mode softening [inset Fig. 2(c)] until it saturates near 30 T. That the majority of vibrational bands are sensitive to applied field [15] is indicative of local structure deformations on approach to the magnetic transition.

To quantify changes in the vibrational properties of $Mn[N(CN)_2]_2$ with magnetic field, we integrate the absolute value of the absorption difference as $\int_{\omega_1}^{\omega_2} |\alpha(B) - \alpha(0\ \text{T})| d\omega$ and plot these quantities along with the magnetization [Fig. 2(d)]. The field-induced spectral changes grow with increasing field and saturate near 30 T where the transition from canted antiferromagnetic to fully polarized state is complete. In general, magnetoelastic phenomena originate from the magnetic state dependence of the elastic properties, which can vary with magnetization intensity and orientation [19]. For instance, in magnetic alloys, the relationship between volume magnetostriction and magnetization goes as $\Delta V/V \sim [M(B)]^2$ [20]. Lattice constants in complex oxides such as $BaCo_2V_2O_8$ also display similar dependence [21]. Our work is different in that we employ local probe (rather than bulk) techniques to uncover the microscopic aspects of the local lattice distortion [22]. Comparison of the data in Fig. 2(d) shows that $Mn[N(CN)_2]_2$ is an example of a molecule-based magnet where the field-induced frequency shifts go as $[M(B)]^2$, an indication of dominant exchange effects [21,23,24]. The strong correlation between phonon behavior and the square of the magnetization suggests that lattice flexibility plays an important role in establishing the fully polarized high-field state. Similar measurements on isostructural $Cu[N(CN)_2]_2$ [25] show no changes within our sensitivity, indicating that the lattice is rigid with field. These control experiments demonstrate that magnetoelastic coupling in $Mn[N(CN)_2]_2$ is associated with the collective phase transition at 30.4 T.

Our spectroscopic measurements reveal that although many infrared-active phonons are sensitive to applied field and display a similar dependence on B, some changes are more important than others. We use relative absorption difference $|\Delta\alpha|/\alpha$ to quantify the relevance of each mode and the local lattice distortion that it represents. The features at 108, 79, and 272 cm^{-1} display the largest changes ($\simeq 29\%$, 12%, and 7% in a 35 T field, respectively). The two leading modes involve Mn displacements in a shearinglike pattern along b (108 cm^{-1}) and a

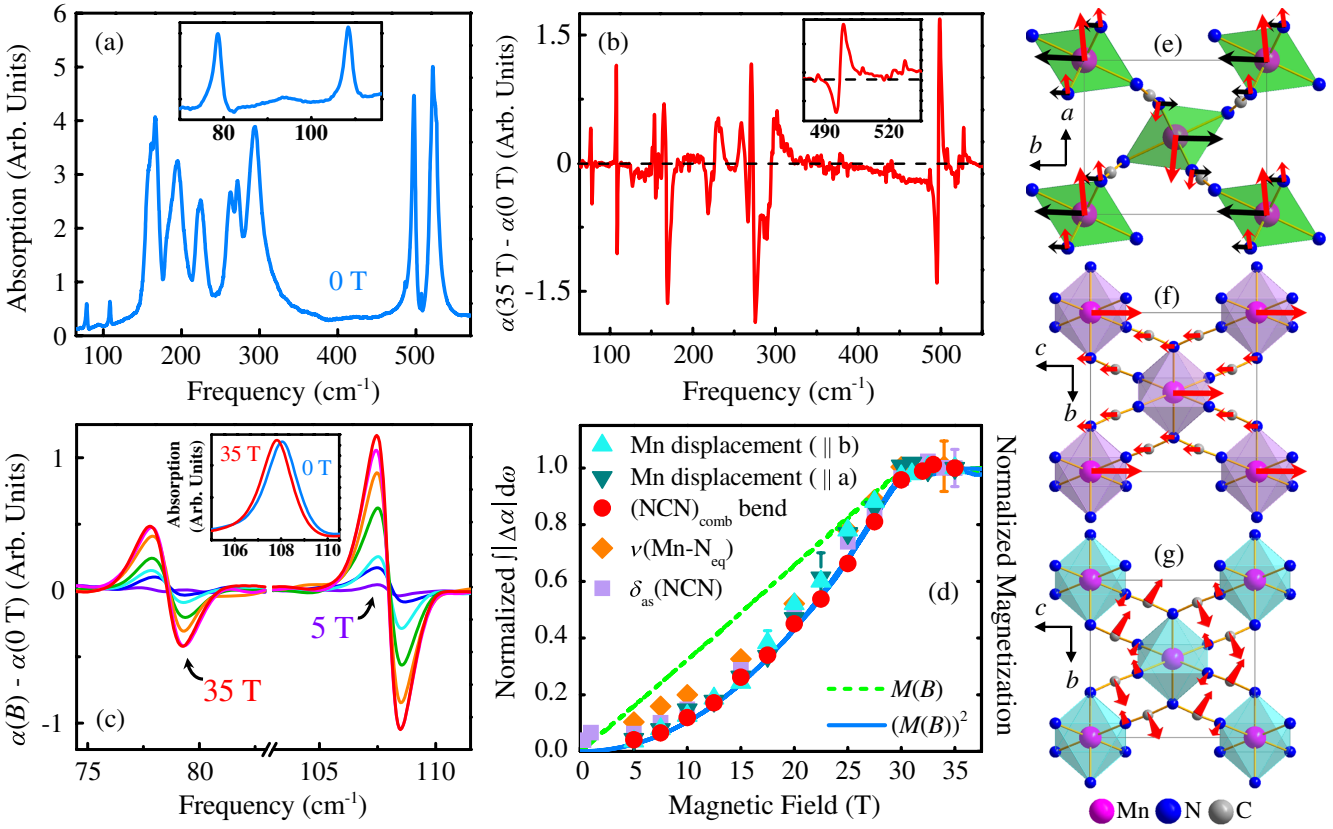

FIG. 2 (color online). (a) Far infrared absorption spectrum of $Mn[N(CN)_2]_2$. Inset: close-up view of the two low-frequency Mn displacement modes. (b) Absorption difference spectrum at $B = 35$ T. Inset: close-up view of the absorption difference in the NCN bending regime. (c) Close-up view of the absorption difference spectrum for the 79 and 108 cm^{-1} lattice modes at 5, 10, 15, 20, 25, 30, and 35 T. The inset highlights the absolute absorption at 0 and 35 T for the 108 cm^{-1} peak. (d) Integrated absolute absorption difference for several characteristic features as a function of applied field compared with magnetization and the square of the magnetization. The data are normalized to 35 T. Both fundamental and combination bands (for instance, the $(NCN)_{comb}$ bend) show similar dependence on field [15]. [(e), (f), (g)] Schematic view of representative displacement patterns as predicted by lattice dynamics calculations. Panel (e) shows the calculated Mn displacement patterns that we assign to the 79 and 108 cm^{-1} peaks, panel (f) displays $\nu(Mn\text{-}N_{eq})$ attributed to the 272 cm^{-1} peak, and panel (g) shows the in-plane asymmetric $\delta_{as}(NCN)$ bend that corresponds to the 497 cm^{-1} peak. All data were taken at 4.2 K.

(79 cm^{-1}) axes, respectively. The next tier contribution (a $Mn\text{-}N_{eq}$ vibration with a 7% change at 272 cm^{-1}) also mainly involves Mn motion but along the c axis. All three modes soften with increasing field. Figures 2(e)–2(g) display schematic views of these displacement patterns along with an example of pure ligand mode motion at 497 cm^{-1}, which has a 5% change in a 35 T field.

A natural framework for understanding the magnetoelastic effect in $Mn[N(CN)_2]_2$ involves local lattice deformations that modify spin exchange interactions to compensate for the increased magnetic energy in the fully polarized state. An analysis of the absorption difference spectra shows that phonons involving mainly Mn centers generally soften with field, and the ligand bands, on the contrary, tend to harden on approach to the transition (Table S1, [15]). This behavior points to a more relaxed MnN_6 octahedra (i.e., less strained bond lengths and equally distributed local angles) and slightly compressed N-C-N linkages in the high-field state. On the basis of the size of $|\Delta\alpha|/\alpha$ through the 30.4 T magnetic quantum critical transition, the distortion primarily affects the 108 cm^{-1} Mn shearing mode along b (with a 29% change). A similar displacement pattern along a (as represented by the 79 cm^{-1} mode and its 12% change) is a large secondary effect. The predominance of low-frequency features in this analysis is indicative of either a real space Mn displacement along b and a or a more complicated distortion of the MnN_6 cage. The magnetoinfrared spectra provide no evidence for high-field symmetry breaking [Fig. 2(c)], a finding that rules out simple transition-metal displacement and also the possibility of a high-field ferroelectric state [12]. In other words, our data indicate that if Mn displacement is present, it is rather small. We therefore conclude that the primary local lattice distortions through the 30.4 T magnetic quantum phase transition involve deformations of the Mn environment, specifically distortions to the MnN_6 octahedral cage.

Examination of the high-field data shows that several ligand bands are sensitive to the 30.4 T quantum critical

transition as well. Although these changes are not large in terms of $|\Delta\alpha|/\alpha$ (Table S1, [15]), they provide additional information about structural flexibility in $Mn[N(CN)_2]_2$. One mechanistic candidate advanced by our first-principles calculations and supported by variable temperature structure work [10] is MnN_6 counterrotation about the c axis (Fig. S2(b), [15]). Analysis of the spectral changes suggests that this is a reasonable model that brings the various MnN_6 and ligand bends together—with the caveat that the MnN_6 octahedra are flexible during counterrotation due to the three-dimensional network. Importantly, the lowest frequency Raman-active mode has a displacement pattern that mirrors the predicted octahedral counterrotation, providing a natural distortion pathway for the system [26]. Comparison of the relaxed structures in the antiferromagnetic and ferromagnetic states suggests that the rotation will be less than 1°.

The magnetic ground state in metal dicyanamides is well-known to arise from a delicate balance between competing antiferromagnetic and ferromagnetic superexchange interactions [9], with exchange strength depending upon magnetic orbital overlap in the metal-ligand-metal linkage, which in turn varies with bond angles and distances [27]. In general, the total spin exchange J can be expressed as a sum of J_{FM} and J_{AFM}, where J_{FM} is the ferromagnetic contribution and J_{AFM} is the antiferromagnetic term [28]. Here, $J_{AFM} \sim t^2/U_{eff}$, where t is the overlap integral and U_{eff} is the effective on-site Coulomb repulsion [28]. As the field-driven magnetic quantum phase transition forces the system to adopt a fully polarized spin alignment, the energy can be reduced by lattice distortions that effectively decrease t. This reduces J_{AFM} and, consequently, the overall J value. Within this picture, MnN_6 counterrotation occurs to lower the total energy of the paramagnetic state forced upon the system by the external magnetic field. Using the prior result [10] that the octahedral tilt is 25.2° at 4.6 K and $B = 0$ T, driving the system into the high-field state yields (for instance) poorer t_{2g} (metal)-π_y (ligand) overlap and a slight increase in the tilting angle [29,30]. Thus, one might speculate that the MnN_6 octahedra counterrotate to reduce J_{AFM} in the high-field state. Perhaps the simplest experimental verification of MnN_6 tilting can be found in the field-induced hardening of the NCN bending modes, although our calculations show that J_{FM}-J_{AFM} is rather small. Of course an important angular effect that influences the magnetic properties of $Mn[N(CN)_2]_2$ is distortion of the MnN_6 octahedra as discussed above. Softening of the 272 cm^{-1} Mn-N_{eq} stretching mode provides support for this process since an increase in the N_{eq}-Mn-N_{eq} angle is consistent with relaxed c-directed Mn motion in the equatorial plane. The resulting decrease in the supplementary angle blue shifts the 224 cm^{-1} ν(Mn-N_{eq}) ab-plane displacement mode (see [15]). Thus, the field-induced local structure changes around the transition-metal center and to the ligand exchange pathway reinforce the magnetic aspects of the transition.

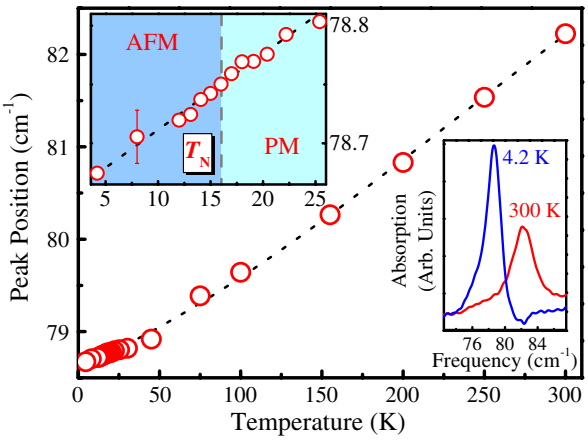

FIG. 3 (color online). Representative peak position vs temperature trend for the 79 cm^{-1} Mn displacement mode. This feature displays one of the largest field-induced changes. The dashed line guides the eye. Upper inset: frequency change through the 15.85 K Néel transition. The trend is monotonic through T_N. The shaded regions visually separate the AFM and PM phases. Lower inset: absolute absorption of this lattice mode.

Motivated by the discovery of magnetoelastic coupling through the 30.4 T quantum critical transition, we sought to expose local lattice distortions through the 15.85 K paramagnetic → canted antiferromagnetic transition [10]. Our measurements reveal, however, only gradual frequency shifts over the temperature range of investigation with no anomalies at T_N (Fig. 3). This indicates that the development of long-range antiferromagnetic order in $Mn[N(CN)_2]_2$ takes place with no significant phonon anomalies (and no substantial lattice involvement). More broadly, it demonstrates that while spin-lattice interaction is inherently rather small in this material, the presence of a collective magnetic transition that switches the system between two different magnetic states with simultaneous, compulsory adjustment of the superexchange interactions can strongly amplify the effect [31]. This finding is reinforced by our high-field data on isostructural $Cu[N(CN)_2]_2$ and suggests that collective transitions can be used to control the interplay between charge, structure, and magnetism.

To summarize, we report the discovery of a magnetic quantum critical transition in $Mn[N(CN)_2]_2$ and the magnetostructural coupling associated with it. In addition to revealing how and why the magnetic quantum critical transition amplifies spin-lattice interactions, our work indicates the need to examine magnetostriction effects in other magnetic materials that have flexible exchange pathways. These findings also illustrate how external stimuli such as magnetic field and temperature in combination with low-energy scale molecule-based materials can be used to uncover microscopic aspects of quantum phase transitions that are elusive in high-energy scale systems like the oxides [13].

Research supported by the U.S. Department of Energy, Office of Basic Energy Sciences, Division of Materials

Sciences and Engineering under Award DE-FG02-01ER45885 (J. L. M., UT), the NHMFL, and Office of Science laboratory under DE-AC02-06CH11357 (J. A. S.) and by the Division of Materials Research at the National Science Foundation under DMR-1005825 (J. L. M., EWU), DMR-0654118 (NHMFL), the computing resources of the NERSC and NCSU HPC centers, and the State of Florida (NHMFL). We thank R. K. Kaul, D. Smirnov, and X. S. Xu for useful discussions.

*Present address: Department of Physics and Astrophysics, University of North Dakota, Grand Forks, North Dakota 58202, USA.

[1] S. Sachdev, *Quantum Phase Transitions* (Cambridge University Press, Cambridge, England, 2011), 2nd ed.; S. E. Sebastian N. Harrison, C. D. Batista, L. Balicas, M. Jaime, P. A. Sharma, N. Kawashima, and I. R. Fisher, Nature (London) **441**, 617 (2006); P. Gegenwart, Q. Si, and F. Steglich, Nat. Phys. **4**, 186 (2008); R. Coldea, D. A. Tennant, E. M. Wheeler, E. Wawrzynska, D. Prabhakaran, M. Telling, K. Habicht, P. Smeibidl, and K. Kiefer, Science **327**, 177 (2010).

[2] P. Gegenwart, J. Custers, C. Geibel, K. Neumaier, T. Tayama, K. Tenya, O. Trovarelli, and F. Steglich, Phys. Rev. Lett. **89**, 056402 (2002).

[3] P. A. Goddard *et al.*, New J. Phys. **10**, 083025 (2008).

[4] J. L. Musfeldt, L. Vergara, T. Brinzari, C. Lee, L. Tung, J. Kang, Y. Wang, J. Schlueter, J. Manson, and M.-H. Whangbo, Phys. Rev. Lett. **103**, 157401 (2009).

[5] J. Schnack *et al.*, Phys. Rev. B **73**, 094401 (2006).

[6] M. Jaime, R. Daou, S. A. Crooker, F. Weickert, A. Uchida, A. E. Feiguin, C. D. Batista, H. A. Dabkowska, and B. D. Gaulin, Proc. Natl. Acad. Sci. U.S.A. **109**, 12404 (2012).

[7] T. Okubo, S. Chung, and H. Kawamura, Phys. Rev. Lett. **108**, 017206 (2012); A. B. Butenko, A. A. Leonov, U. K. Rößler, and A. N. Bogdanov, Phys. Rev. B **82**, 052403 (2010).

[8] E. Coronado and P. Day, Chem. Rev. **104**, 5419 (2004); J. S. Miller, Chem. Soc. Rev. **40**, 3266 (2011).

[9] J. L. Manson, C. R. Kmety, A. J. Epstein, and J. S. Miller, Inorg. Chem. **38**, 2552 (1999); A. Lappas, A. S. Wills, M. A. Green, K. Prassides, and M. Kurmoo, Phys. Rev. B **67**, 144406 (2003).

[10] C. R. Kmety, Q. Huang, J. Lynn, R. Erwin, J. Manson, S. McCall, J. Crow, K. Stevenson, J. Miller, and A. Epstein, Phys. Rev. B **62**, 5576 (2000); J. L. Manson, C. R. Kmety, F. Palacio, A. J. Epstein, and J. S. Miller, Chem. Mater. **13**, 1068 (2001).

[11] J. F. Scott, Rev. Mod. Phys. **46**, 83 (1974); P. Bouvier and J. Kreisel, J. Phys. Condens. Matter **14**, 3981 (2002); A. Palewicz, R. Przeniosło, I. Sosnowska, and A. W. Hewat, Acta Crystallogr. Sect. B **63**, 537 (2007); X. J. Liu, Y. Moritomo, T. Matsuda, H. Kamioka, H. Tokoro, and S.-i. Ohkoshi, J. Phys. Soc. Jpn. **78**, 013602 (2009).

[12] N. A. Benedek, A. T. Mulder, and C. J. Fennie, J. Solid State Chem. **195**, 11 (2012) and references therein.

[13] F. F. Balakirev, J. Betts, A. Migliori, I. Tsukada, Y. Ando, and G. Boebinger, Phys. Rev. Lett. **102**, 017004 (2009); H. Nojiri, Y. Shimamoto, N. Miura, M. Hase, K. Uchinokura, H. Kojima, I. Tanaka, and Y. Shibuya, Phys. Rev. B **52**, 12749 (1995); O. Kondo, M. Ono, E. Sugiura, K. Sugiyama, and M. Date, J. Phys. Soc. Jpn. **57**, 3293 (1988).

[14] Y. Tokunaga, S. Iguchi, T. Arima, and Y. Tokura, Phys. Rev. Lett. **101**, 097205 (2008); Y. J. Choi, C. L. Zhang, N. Lee, and S.-W. Cheong, Phys. Rev. Lett. **105**, 097201 (2010).

[15] See the Supplemental Material at http://link.aps.org/supplemental/10.1103/PhysRevLett.110.237202 for details.

[16] The strongest near-neighbor magnetic-exchange interaction proceeds through the Mn-N≡C-N-Mn linkage. Here, we employ a single J spin Hamiltonian of the form $\mathcal{H} = -J\sum_{\langle i,j\rangle}\mathbf{S}_i \cdot \mathbf{S}_j - g\mu_B B\sum_i S_i^z$. The definition of J used in Ref. [10] differs by a factor of 2 from our usage.

[17] T. Fries, Y. Shapira, F. Palacio, M. Morón, G. McIntyre, R. Kershaw, A. Wold, and E. McNiff, Phys. Rev. B **56**, 5424 (1997).

[18] M. Kuhn and R. Mecke, Chem. Ber. **94**, 3010 (1961); H. Köhler, A. Kolbe, and G. Lux, Z. Anorg. Allg. Chem. **428**, 103 (1977); B. Jürgens, H. A. Höppe, and W. Schnick, Solid State Sci. **4**, 821 (2002).

[19] *Magnetism: Fundamentals*, edited by E. du Trémolet de Lacheisserie, D. Gignoux, and M. Schlenker (Springer Science, Boston, 2005).

[20] Volume (exchange) magnetostriction arises due to the volume dependence of exchange integral (Ref. [19]); P. P. M. Meincke, Can. J. Phys. **48**, 859 (1970); G. Hausch, Phys. Status Solidi (a) **18**, 735 (1973); Y. Nakamura, J. Magn. Magn. Mater. **31–34**, 829 (1983).

[21] S. Kimura *et al.*, J. Phys. Soc. Jpn. **79**, 043706 (2010).

[22] M. B. Smith, K. Page, T. Siegrist, P. L. Redmond, E. C. Walter, R. Seshadri, L. E. Brus, and M. L. Steigerwald, J. Am. Chem. Soc. **130**, 6955 (2008).

[23] E. Callen and H. B. Callen, Phys. Rev. **139**, A455 (1965).

[24] E. Granado, A. García, J. Sanjurjo, C. Rettori, I. Torriani, F. Prado, R. Sánchez, A. Caneiro, and S. Oseroff, Phys. Rev. B **60**, 11879 (1999).

[25] C. R. Kmety, J. L. Manson, S. McCall, J. E. Crow, K. L. Stevenson, and A. J. Epstein, J. Magn. Magn. Mater. **248**, 52 (2002). Our measurements were done in the far infrared.

[26] A direct check of the low-frequency Raman mode is impossible at this time due to probe limitations at the NHMFL.

[27] J. B. Goodenough, *Magnetism and the Chemical Bond* (Wiley, New York, 1963).

[28] P. W. Anderson, *Solid State Physics* (Academic Press, New York and London, 1963), Vol. 14, pp. 99; M.-H. Whangbo, H.-J. Koo, and D. Dai, J. Solid State Chem. **176**, 417 (2003).

[29] A. Escuer, F. A. Mautner, N. Sanz, and R. Vicente, Inorg. Chem. **39**, 1668 (2000).

[30] The tilt angle is defined as the angle between the equatorial plane of the MnN_6 octahedron and the ac plane [10].

[31] Magnetic field induces twice the change in $\langle \mathbf{S}_i \cdot \mathbf{S}_j \rangle$ compared with that of temperature [19,23].